Mechanical Coupling of 2D Resonator Arrays for MEMS Filter Applications

Dana Weinstein, Sunil A. Bhave
Cornell University
Ithaca, NY, USA
dw222@cornell.edu

Masahiro Tada, Shun Mitarai, Shinya Morita, Koichi Ikeda
Sony Corporation
Kanagawa, Japan

Abstract— **This paper presents a study of mechanical coupling in 2D resonator arrays for filter applications. A robust coupling design for 2D array filters, comprised of weak coupling in one dimension and strong coupling in the second, is demonstrated experimentally and compared with weakly coupled and electrically summed 2D resonator array filters. Effects of inherent disorder in resonator arrays due to fabrication variations are minimized in this mechanical coupling scheme, averaging over resonator mismatch to form a smooth pass-band. The strongly-coupled 2D filter improves insertion loss and ripple without degradation in filter shape factor or stop-band rejection relative to its 1D counterpart.**

I. Introduction

Micro-Electromechanical resonators, with quality factors (Q) often exceeding 10,000, have emerged as leading candidates for on-chip versions of high-Q resonators used in wireless communications systems. Much of current MEMS resonator research focuses on channel-select filters for radio front-ends. One-dimensional and bridged arrays of MEMS resonators have been studied extensively to form narrow bandwidth filters at low MHz frequencies. To improve insertion loss, multiple resonators have been strongly coupled to increase transduction area in two-pole filters [1]. Alternatively, sets of 1D filters coupled electrically in parallel have been proposed and demonstrated [2]. However, pure electrical coupling does not ensure a coherent summation of the filter passband due to small variations between each electrically parallel 1D filter. Some strong mechanical coupling is therefore required to drive an array of 1D filters coherently.

II. Theoritical Motivation

Though two-pole filters currently dominate RF MEMS filter research, there is an impetus to extend to multi-pole filters. As shown by Wang *et al* [3], increasing the number of resonators in a 1D filter improves both pass-band shape factor and stop-band rejection. However, spatial decay in the resonators and fabrication variations result in increased insertion loss and distortion in the passband as more resonators are added to the 1D array. This phenomenon has previously been investigated by Castanier and Pierre [4], using classical perturbation theory to model the effects of both dissipation and variations on 1D filters.

To improve this passband distortion, Judge *et al* [5] proposed a 2D coupling which averages out the stochastic resonator characteristics. The design strongly couples an array of identical 1D filters, generating a two-dimensional matrix of resonators which are coupled weakly in one direction and strongly in the other (Figure 1).

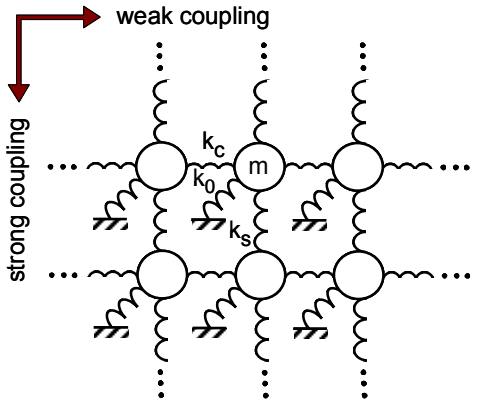

Figure 1. 2D mechanical coupling configuration under investigation to reduce effective resonator variations. Here, the coupling stiffness $k_C \ll k_S$.

The weak coupling (k_C) defines the filter passband, as in the case of the 1D filter. The number of resonators in the weak coupling direction therefore defines the number of poles in the passband. The strong coupling (k_S) averages variations in the resonators due to fabrication tolerances. If $k_C \ll k_S$, and N_S the number of resonators in the strong coupling direction, then the effective standard deviation of variations in the resonators is

$$\sigma_{eff} = \frac{\sigma}{\sqrt{N_s/2}} \quad , N_S \text{ even}$$
$$\sigma_{eff} = \frac{\sigma}{\sqrt{(N_s+1)/2}} \quad , N_S \text{ odd.} \qquad (1)$$

The enhanced number of acoustic energy paths in the filter provided by the strong coupling reduces the effect of resonator variations, averaging out stiffness mismatch between resonators, consequently improving passband distortion.

III. Experimental Setup

A. Filter Design

In this study, four resonator coupling configurations are investigated to determine the effectiveness of the 2D strongly coupled array filter. We construct a 1D 4-pole filter (Figure 2a) as a basis of comparison for all 2D filters in the study. The performance of this 1D filter is compared with a set of four 1D 4-pole filters, electrically summed in parallel (Figure 2b), a 2D 4x4 array of resonators, weakly coupled in both directions (Figure 2c), and a 2D 4x4 array of resonators, coupled weakly in one direction and strongly in the other (Figure 2d).

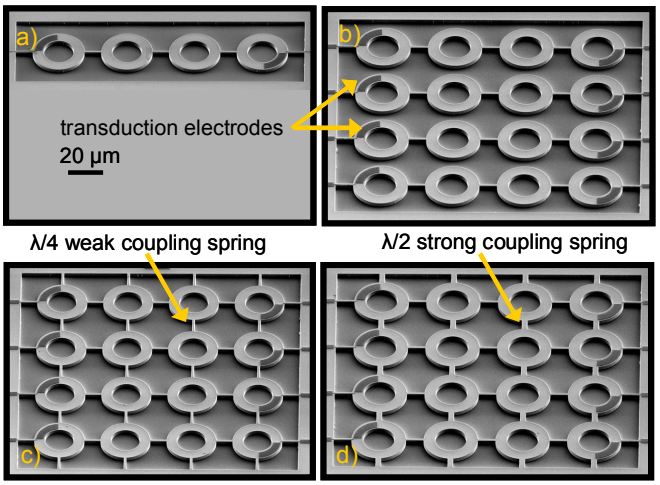

Figure 2. Scanning Electron Micrographs of (a) a 1D 4-pole filter, (b) 4 electrically summed 1D 4-pole filters, (c) a 4x4 array of resonators, coupled weakly in both directions, and (d) a 4x4 array of resonators, coupled weakly in one direction and strongly in the other.

The filters are composed of extensional wine glass ring resonators [6] with a fundamental resonance designed for 500 MHz. The resonators are driven and sensed with lateral dielectric transduction [7]. Soft coupling springs between the resonators, used to define the bandwidth of the filter, are achieved with 2 µm wide beams of quarter wave length matched at 500 MHz. Strong coupling springs used in the proposed strongly coupled array are designed with 4 µm wide beams of half wave length. The resonators are coupled at the quasi-nodes of the extensional wine glass ring mode.

The choice of a resonant mode with 90º rotational symmetry (albeit out-of-phase) enables an ideal 2D coupling for this study. The effective stiffness of the resonator at the coupling point is identical for coupling in both directions, such that the coupling is defined nominally by the dimensions of the coupling beam. This design is chosen for ease of comparison across several filters. However, the restriction on resonator type is not a requirement, and any resonator can be implemented with proper modeling.

B. *Fabrication*

The filters are fabricated in a simple SOI process for lateral dielectric transduction, shown in Figure 3. First, 100 nm of LPCVD stoichiometric silicon nitride are deposited on a 3 µm thick n+ silicon device layer. This dielectric forms the transduction film for the resonators. The nitride is then patterned to provide electrical contact to the device layer for biasing the resonators. 100 nm of LPCVD n+ polysilicon are then deposited and patterned to form the probe pads, routing, and transduction electrodes. The resonator bodies are then defined in a deep reactive ion etch (DRIE) of the silicon device layer. Finally, the resonators are released in HF and critical-point dried (CPD) to prevent stiction.

IV. Experimental Results

A. *Measurement and Calibration*

The filters were characterized in a vacuum RF probe station in a 2-port configuration using GSG probes. Parasitics up to the probe tips were first cancelled with SOLT measurements on a standard calibration substrate. De-embedding was then performed with Cascade WinCal software, using short, open, and through structures fabricated on-chip, but separate from the filters. This de-embedding allows for the cancellation of the large pad capacitance without canceling out any parasitics inherent to the filters themselves, including suspension beam routing and transduction electrodes on the resonators.

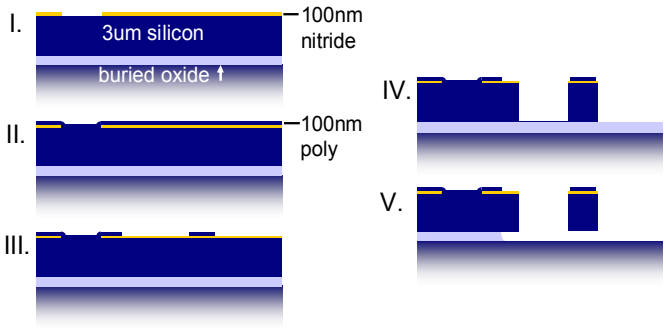

Figure 3. SOI fabrication process for the extensional wine glass ring filters. (I.) A 100 nm silicon nitride film is deposited a on a 3 µm n+ silicon device layer and patterned. (II.) A 100 nm film of n+ polysilicon is deposited, and (III.) patterned to form bond pads, routing, and resonator electrodes. (IV.) The resonator body is defined in a DRIE of the device layer and (V.) released in HF and dried at critical point to avoid stiction.

B. *Wine Glass Ring Resonator*

Figure 4 shows the unterminated S_{21} response of a single wine glass ring resonator, applying a bias voltage of 11 V. 10 resonators were characterized in vacuum, varying in frequency from 511-514 MHz and in electromechanical quality factor (Q_{em}) from 5000 to 8000.

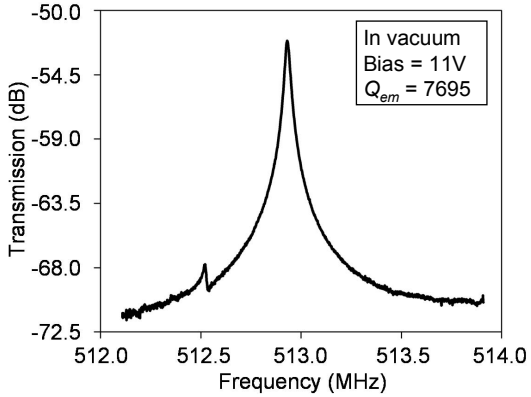

Figure 4. Unterminated S_{21} transmission response of a single wine glass ring resonator.

C. *Filter Performance*

Applying 10 V across the 100 nm nitride transducer, we obtain the frequency response of the 1D 4-pole filter, shown in Figure 5a. The filter has a center frequency of 511 MHz with a 3 dB bandwidth of 1.49 MHz. The Unterminated response clearly shows the four poles defining the filter. Due to fabrication variations, there is a significant distortion to the passband, with a ripple (defined as the maximum peak to minimum trough) of 5.4 dB. The 1D filter frequency response provides a basis of comparison for the rest of the filters in this study.

Figure 5b presents the 50 Ω terminated S_{21} transmission of the 4 electrically summed 1D 4-pole filters (Figure 2b). The increased transduction area of the electrically summed 1D filters improved the insertion loss (IL, defined here at the maximum peak) by 7 dB relative to the single 1D chain. Additionally, the passband flattened to only 1.1 dB ripple, due to the summation of four 4-pole filters, offset in frequency from one another due to fabrication variations. However, these improvements are at the expense of filter shape factor and stop-band rejection. The electrically summed array filter has a 3 dB – 8 dB shape factor of 2.19 – a 30% degradation from the single 1D chain shape factor of 1.68. Furthermore, the stop-band rejection of the electrically summed filter reduces to 11.1 dB from 16.7 dB in the case of the single chain.

We next inspect the case of the 4x4 array of resonators, weakly coupled in both directions, shown in Figure 5c. This 2D array has too many resonant modes to be considered a filter. However, the behavior of this filter demonstrates that the strong coupling in the next filter is indeed strong enough relative to the weakly coupled direction.

Finally, we observe the effects of coupling a 4x4 2D array of resonators weakly in one direction (defining the resonant modes which contribute to the passband) and strongly in the other direction (averaging out fabrication variations). The unterminated frequency response of this filter is presented in Figure 5d. As in the case of the electrically summed filters, the insertion loss improves due to increased transduction area. It should be noted that the expected improvement in IL for both the electrically summed filter and the strongly coupled 2D filter is 13.9 dB due to the 4x increase in electrode area. However, the filters show an IL increase of only 7-8 dB. This discrepancy is attributed to the process variations, including non-uniformity of the nitride thickness and polysilicon resistivity.

It should be noted that the bandwidth of the strongly coupled filter (1.1 MHz) is narrower than that of its 1D counterpart (1.49 MHz). The bandwidth narrowing corresponds to an effective stiffening of the resonator due to the non-ideal strong coupling beams. It can be compensated using different strong coupling designs (dependent on the geometry of the resonators comprising the filter) or simply by changing the effective stiffness of the soft coupling beams in the array.

Additionally, there is a frequency shift in the passband of about 1 MHz relative to the 1D filter. This frequency shift can be observed in the frequency response of all the 2D arrays, and is attributed variations in DRIE device layer etch rates for small and large open areas on a single mask. In the case of the 2D strongly coupled array, the center frequency shift is due to both etch rate effects and due to resonator mass loading from the 4 μm wide strong coupling beams.

The ripple of the 2D strongly coupled filter improves from 5.4 dB to 4.2 dB relative to the 1D 4-pole filter. This corresponds to a 22% improvement in the passband ripple.

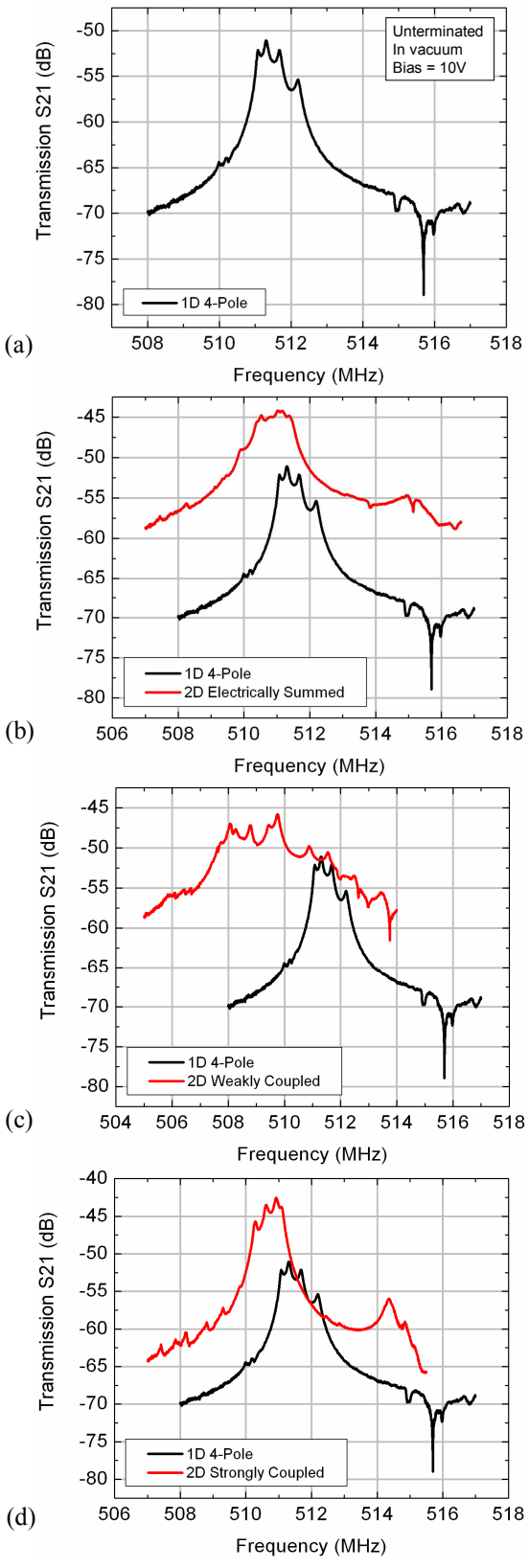

Figure 5. Unterminated S_{21} transmission plot of (a)1D 4-pole filter, (b) comparison of 1D filter with 4 electrically summed 1D filters, (c) comparison of 1D filter with 4x4 2D weakly coupled array, and (d) comparison of 1D filter with 4x4 2D strongly coupled array.

The improvement in passband distortion does not sacrifice filter stop-band rejection and shape factor. The stop-band rejection increases from 16.7 dB to 17.6 dB while the filter shape factor (3 dB–8 dB) decreases from 1.68 to 1.55 for the 2D strongly coupled filter relative to the 1D filter. These 5-8% improvements do not make the observed trend definitive. A larger number of 2D strongly coupled filters must be tested in order to determine if the strong coupling configuration actually improves these filter characteristics. It is evident, however, that the 2D coupling improves distortion in the filter passband without degrading filter performance.

V. CONCLUSION

In this work, we demonstrated the effectiveness of a 2D mechanical coupling configuration for filters in reducing passband distortion due to micro-fabrication variations. A 2D filter comprised of a 4x4 array of bulk-mode wine glass ring resonators was demonstrated at 511 MHz. The 2D coupling provided a 22% improvement in unterminated passband ripple relative to its 1D counterpart, without degradation in stop-band rejection or shape factor. This strong mechanical coupling provides a more robust solution to fabrication variations than the electrically summed filter, which suffered a 33% decrease in stop-band rejection and a 30% increase in shape factor relative to the 1D filter. For reference, Table 1 quantifies the transmission response of the three filters under examination.

In addition, the electrically summed filter demonstrates unpredictable bandwidth from filter to filter, due to its sensitive dependence on fabrication variations. Though the electrically summed filter produced a flatter passband than the strongly coupled filter in the case of the 4x4 array, we can simply couple more resonators in the stiff direction to improve passband distortion and insertion loss, without degradation of filter performance.

The 2D strong mechanical coupling configuration examined in this work can be implemented with any resonators in any fabrication process, providing more reliable and repeatable high-performance MEMS filters.

TABLE I. SUMMARY OF UNTERMINATED FILTER PERFORMANCE

	1D 4-Pole Filter	2D Electrically Summed Filter	2D Strongly Coupled Filter
Insertion Loss[a]	-51.1 dB	-44.2 dB	-42.5 dB
3dB Bandwidth	1.49 MHz	1.56 MHz	1.1 MHz
Stop-Band Rejection	16.7 dB	11.1 dB	17.6 dB
Shape Factor (3 dB – 8 dB)	1.68	2.19	1.55
Ripple[b]	5.38 dB	1.18 dB	4.22 dB

a. 50 Ω terminated, defined from maximum peak in passband.
b. 50 Ω terminated, defined from maximum peak to minimum trough.

REFERENCES

[1] J.R. Clark, M. Pai, B. Wissman, G. He, W..-T. Hsu, "Parallel-coupled square-resonator micromechanical filter arrays," Proceedings of the 2006 IEEE International Frequency Control Symposium, pp.485 - 490.

[2] P.J. Stephanou, G. Piazza, C.D. White, M.B.J. Wijesundara, A.P. Pisano, "mechanically coupled contour mode piezoelectric aluminum nitride MEMS filters," 19th IEEE International Conference on Micro Electro Mechanical Systems (MEMS) 2006, pp.906-909.

[3] K. Wang, C.T.-C. Nguyen, "High-order medium frequency micromechanical electronic filters," Journal of Microelectomechanical Systems, **8**(4), pp. 534-557 (1999).

[4] M.P. Castanier and C. Pierre, "Individual and interactive mechanisms for localization and dissipation in a mono-coupled nearly-periodic structure," Journal of Sound and Vibration **168**(3), pp.479-505 (1993).

[5] J.A. Judge, B.H. Houston, D.M. Photiadis, P.C. Herdic, "Effects of disorder in one and two dimensional micromechanical resonator arrays for filtering," Journal of Sound and Vibration **290**(3-5), pp.1119-1140 (2006).

[6] Y. Xie, S.-S. Li, Y.-W. Lin, Z. Ren, C.T.-C. Nguyen, "UHF Micromechanical Extensional Wine-Glass Mode Ring Resonator," IEEE International Electron Device Meeting 2003, pp.953-956.

[7] D. Weinstein, H. Chandrahalim, L.F. Cheow, S.A. Bhave, "Dielectrically transduced single-ended to differential MEMS filter," IEEE International Solid-State Circuits Conference (ISSCC) 2006, pp.1236-1243.